Journal of Power Sources 478 (2020) 228991

Contents lists available at ScienceDirect

Journal of Power Sources

journal homepage: www.elsevier.com/locate/jpowsour

Stochastic capacity loss and remaining useful life models for lithium-ion batteries in plug-in hybrid electric vehicles

Andrew Chu [a,1], Anirudh Allam [b,1], Andrea Cordoba Arenas [c,1], Giorgio Rizzoni [c,1], Simona Onori [b,*,1]

[a] The Nueva School, San Mateo, CA 94403, USA
[b] Energy Resources Engineering Department, Stanford University, Stanford, CA 94305, USA
[c] Center for Automotive Research and Department of Mechanical and Aerospace Engineering, The Ohio State University, Columbus, OH 43212, USA

ARTICLE INFO

Keywords:
Lithium-ion battery
Capacity estimation
Remaining useful life prediction
State of charge
Resistance estimation
Particle filter
Electrified vehicles

ABSTRACT

This paper proposes and validates a stochastic prognostic model for capacity loss and remaining useful life (RUL) in lithium-ion pouch cells with graphite anodes and NMC–LMO cathodes. The model was developed using data from an experimental campaign which studied the effect of C-rate, minimum SOC, temperature, and charge-depleting usage on aging in plug-in hybrid electric vehicle (PHEV) batteries. The proposed algorithm estimates capacity loss and RUL as a function of resistance and operating conditions including charge sustaining/depleting use and temperature, and its stochastic nature is able to capture the variability of the data. The battery resistance is estimated using a particle filter developed for an experimentally validated equivalent circuit battery model. The particle filter is designed to perform combined estimation of State of Charge and internal resistance, which is used as an input to the stochastic capacity loss model. Finally, the stochastic model predicts the capacity loss with a root mean square error (RMSE) of less than 1% and RUL with an RMSE of 1.6 kAh, and can be integrated into on-board battery management systems in PHEV to monitor the health of lithium-ion batteries.

1. Introduction

Although the global market for hybrid and electric vehicles is growing, a key improvement necessary to accelerate the adoption of these vehicles is to optimize the efficiency with which they are used. The battery pack is the most expensive component of the vehicle and it is sometimes replaced too early or used inefficiently as there is no accurate way to evaluate when it has reached its end of life. The industry benchmark is that end of life occurs when the battery's capacity is at 80% of its original value. Only by means of an in-laboratory capacity test the battery capacity can be attained and assessed throughout its life; direct on-board capacity measurements are not feasible. Due to this challenge, on-board battery management systems (BMS) often use a crude estimate of when a battery has reached end of life by simply counting up to a pre-determined ampere-hour throughput or discharge cycles. This method is an inaccurate reflection of capacity as it does not factor in how drivers use their vehicles with differing frequency and aggressiveness or exogenous environmental parameters such as the climate or local driving conditions.

A more accurate and versatile method to predict the remaining useful life (RUL) in lithium-ion batteries could allow consumers to use their batteries for several years longer (through ensuring that batteries are only replaced when end of life has been reached) and also increase understanding of what operating conditions affect the aging process the most. Semi-empirical and empirical models for capacity loss are currently used in BMS applications [1–3]. Although operating conditions such as state of charge (SOC) and C-rate are often used for empirical models of capacity loss, no such models have been stochastic [4,5]. Notably, a stochastic model such as the one proposed in this paper can offer a better and more useful estimate of capacity loss since it is able to effectively capture the intrinsic aleatory nature of aging data. In addition, a growing area of battery prognostics involves machine learning techniques which often can predict capacity loss accurately from battery operating conditions [6]. However, the black-box nature of machine learning algorithms means that one cannot associate them with underlying physics-based explanations. Moreover, due to their mathematical complexity, such models are hard to implement in the

* Corresponding author.
E-mail address: sonori@stanford.edu (S. Onori).
[1] AC, AA, and SO contributed to the work equally, ACA and GR provided the battery data.

https://doi.org/10.1016/j.jpowsour.2020.228991
Received 7 April 2020; Received in revised form 27 August 2020; Accepted 22 September 2020
Available online 12 October 2020
0378-7753/

limited hardware of automotive BMSs. On the other side of the spectrum, algorithms which have been tailored to be suitable for on-board BMSs are often inaccurate and unable to predict remaining useful life early on in the aging process [7].

This paper describes a novel, stochastic model that can estimate capacity loss and remaining useful life from on-board measurements and on-the-fly calculation of resistance with a given uncertainty. The basis of the model is a square root relationship between capacity and resistance. Previous studies using analytical models have often not considered an expression for capacity as a function of resistance, and even when they have, a square root relationship has never been seen between these two variables [8,9]. Moreover, previous attempts have not established a stochastic and analytical expression to identify a correlation between capacity loss and resistance growth. [10].

Past studies using semi-empirical capacity fade models have demonstrated the necessity for the simple onboard estimation of the model's parameters which can be accomplished without significant new computational infrastructure [11]. Moreover, although probabilistic models have been developed for end of life (EOL) calculation, these algorithms are very computationally intensive and are limited to the scope of EOL [12,13]. The authors do not find probabilistic capacity fade models in the literature. However, there is a precedent for the success of probabilistic aging models as well as models which require online parameter calibration. In addition, Kalman and particle filters are the most common and most effective tools for estimating dynamic battery aging parameters such as SOC [14]. Particle filters, in particular, are commonly used to estimate the change of resistance and capacity over the life of a battery [15].

Further, battery state and parameter estimation algorithms such as Kalman Filters [16–19], Sliding-mode observers [20,21], and particle filters [22,23] have been employed in the literature. In this work, a particle filter is developed for a battery equivalent circuit model capable of combined estimation of SOC and internal resistance. This is then used in the stochastic estimation algorithm of capacity loss. The stochastic feature of the proposed model was developed by fitting a Gaussian distribution to the error of the model and calculating the mean and standard deviation, so a random variable could be stochastically selected from this distribution for every prediction. In this work, the model is trained and validated on a limited experimental data set as well as data generated from a previous model built on that data.

The paper is organized as follows. In Section 2, the experimental campaign as well as the deterministic model which was previously built from this data are presented. In Section 3, an outline of the entire proposed model and its different components are given. In Sections 4 and 5 , the battery model and corresponding particle filter are presented. In Sections 6 and 7, the development and validation of the capacity loss model and the remaining useful life model are described, respectively. Finally, in Section 8, the results of the full proposed model are shown and the overall conclusions are presented in Section 9.

2. Experimental data

The experimental data used in this study was from an aging campaign conducted on graphite–NMC–LMO pouch cells that mimicked the behavior of PHEV batteries [1]. The design of experiments used in this work is tabulated in Table 1 and the specific SOC profile and power micro cycle are provided in Fig. 1. The purpose of the experiments was to determine the effects of the following operating conditions on battery aging: Ratio, minimum SOC (SOC min), charging C-rate, and temperature. For a cell that has spent t_{CD} time in charge-depleting mode (where the car is operating as an electric vehicle and does not use the internal combustion engine) and t_{CS} time in charge-sustaining mode (where the vehicle operates as a hybrid vehicle with a relatively constant SOC), the Ratio of the cell is defined as

$$Ratio = \frac{t_{CD}}{t_{CS} + t_{CD}}. \tag{1}$$

Table 1
The operating conditions for each cell in the experimental campaign. A total of 11 cells of experimental data used in the creation and validation of the model. The acronym CD stands for Charge Depleting mode.

Cell #	Operating mode	Ratio	SOC_{min} [%]	Charging C-rate	Temp [deg C]
2	CD	1	35	C/3	30
3	CD	1	25	C/3	30
4	CD	1	45	C/3	30
5	CD	1	35	3C/2	30
6	CD	1	25	3C/2	30
7	CD	1	45	3C/2	30
8	CD	1	35	5C	30
9	CD	1	25	5C	30
14	Mixed	1/2	35	3C/2	30
15	Mixed	1/4	35	3C/2	30
16	Mixed	1/2	35	3C/2	45

The experimental campaign mimics true PHEV battery usage in several facets. First, the CD and CS operational modes are composed of power micro cycles (as defined by the USABC) which represent actual automotive battery usage [24]. In addition, the SOC_{max} and SOC_{min} describe typical charging and discharge levels used in vehicles and the two experimental temperatures are well within the normal range of operation.

From the experimental campaign, data of percent capacity loss and percent resistance increase as a function of charge throughput was collected. Capacity loss is defined as

$$Q_{loss} = \frac{Q_0 - Q(Ah)}{Q_0} \cdot 100, \tag{2}$$

where Q_0 is the nominal capacity and $Q(Ah)$ is the capacity at the given charge throughput value. Q_{exp} refers to experimental data of capacity loss, defined in the same manner as in (2). Similarly, resistance is defined as

$$R_{inc} = \frac{R(Ah) - R_0}{R_0} \cdot 100, \tag{3}$$

where R_0 is the nominal battery resistance at the beginning of life and $R(Ah)$ is the resistance at the given charge throughput value.

In this study, the data from the experimental campaign was plotted in the form of capacity loss against resistance increase. Visualizing the capacity loss information in such a manner has the advantage of relating a quantity that can be calculated on board (i.e. resistance) with a health-related signal that is not either measurable or directly computed on board. The capacity loss of a given cell as a function of resistance is referred to as $Q_{loss}(R_{inc})$.

In [1], an aging model to predict capacity loss and resistance increase from cell operating conditions was also proposed and experimentally validated. The model is described by the systems of equations in (4), where $Q_{syn}(Ah)$ is the prediction of capacity loss from the semi-empirical model, $a_C(SOC_{min}, Ratio)$ is the capacity severity factor function, $R_{inc}(Ah)$ is the prediction of resistance increase, and $a_R(SOC_{min}, Ratio, CR)$ is the resistance severity factor function. The constants for (4) were calibrated in [1] and displayed in Table 2 for the convenience of the reader.

$$\begin{cases} Q_{syn}(Ah) & = a_C(SOC_{min}, Ratio) \cdot exp\left(\frac{E_{a_c}}{R_g T}\right) \cdot Ah^z \\ a_C(:,:) & = \alpha_c + \beta_c \cdot Ratio^b + \gamma_c \cdot \left(SOC_{min} - SOC_0\right)^c \\ R_{syn}(Ah) & = a_R(SOC_min, Ratio, CR) \cdot exp\left(\frac{E_{a_R}}{R_g T}\right) \cdot Ah \\ a_R(:,:,:) & = \alpha_R + \beta_R \cdot \left(SOC_{min} - SOC_0\right)_R^c + \\ & \quad \gamma_R \cdot \exp\left[d \cdot \left(CR_0 - CR_{eq}\right) + e \cdot \left(SOC_{min} - SOC_0\right)\right] \\ CR_{eq}(Ratio) & = \begin{cases} 0, & Ratio = 0 \\ 1, & Ratio > 0 \end{cases} \end{cases} \tag{4}$$

In this study, to complement the actual experimental aging data, we use the two models described in (4) to generate synthetic capacity

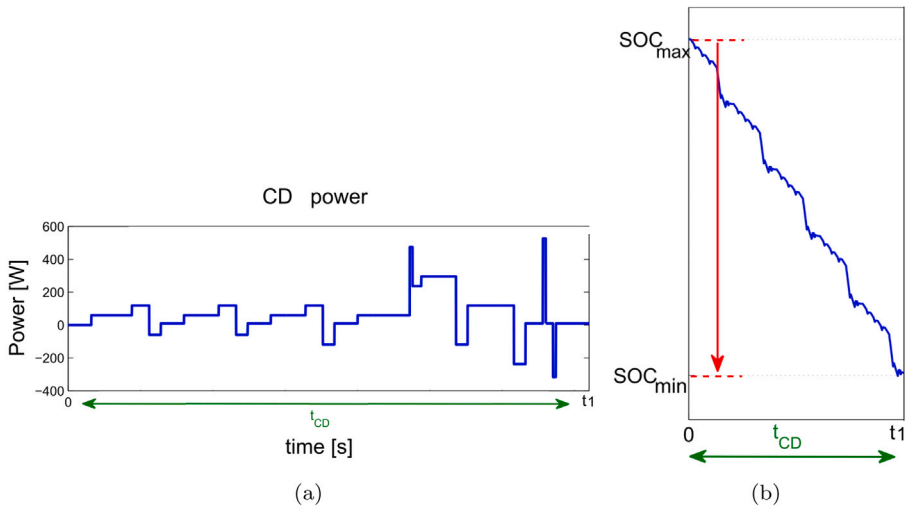

Fig. 1. (a), (b) show the typical power and corresponding SOC profiles of Charge Depleting (CD) mode, where the SOC_{max} is 95 and SOC_{min} depends on the specific experiment and can assume values of 25, 35, or 45. Figures are adapted from [1]. Further details regarding the aging profiles and conditions of the experiments may be found in the aforementioned reference.

Table 2
Parameters in (4) as calibrated from experimental results so as to fit the resistance increase and capacity loss data in [1].

Notation	Value	Description
α_c	137	Dimensionless constant
β_c	420	Dimensionless constant
γ_c	9610	Dimensionless constant
c	0.34	Dimensionless constant
c	3	Dimensionless constant
z	0.48	Dimensionless constant
E_{a_c}	22 406 [J mol^{-1}]	Activation energy of the capacity loss model
α_R	3.2×10^5	Dimensionless constant
β_R	1.3674×10^9	Dimensionless constant
γ_R	3.6342×10^3	Dimensionless constant
c_R	5.45	Dimensionless constant
d	0.9179	Dimensionless constant
e	1.8277	Dimensionless constant
CR_0	5	Dimensionless constant
SOC_0	0.25	Dimensionless constant
E_{a_R}	51 800 [J mol^{-1}]	Activation energy of the resistance growth model
R_g	8.314 [J K^{-1} mol^{-1}]	Universal gas constant

loss data Q_{syn}. Note that Q_{syn} is a function of Ah, as previously defined in the creation of the model in [1], while Q_{pred}, the proposed model's prediction of capacity loss, is a function of R_{inc}. For convenience, the nomenclature being used in the paper is given in Table 3.

The Q_{syn} data (which is used to develop the model proposed in this study) was generated under operating conditions either identical to or within the range used in the previous experimental campaign. These ranges are described below:

1. SOC_{min} (either 25%, 35%, or 45%)
2. Ratio (either $1, 1/2$, or $1/4$)
3. Temperature (between 30–45 °C, with increments of 1 °C)
4. C-rate (between $0.4C$ and $5C$, with increments of $0.2C$)
5. Ampere-hour throughput (between 0–30,000 Ah, with increments of 500 Ah)

Note that C-rate is only used in (4) for calculating resistance, as it plays no role in estimating capacity loss. Eq. (4) was used to calculate the resistance increase and capacity loss at 500 Ah increments of a hypothetical battery cell which had characteristics from the list above. A total of 257,664 synthetic Q_{syn} data points were generated for each Ratio; this number is simply the amount of unique combinations of the possible SOC_{min}, Ratio, temperature, C-rate, and Ampere-hour throughput values defined previously. After generating this data, any

Table 3
Nomenclature.

Notation	Description
Q_{exp}	Capacity loss data from the experimental campaign, as a function of resistance
Q_{syn}	Generated capacity loss data from the model described by Eqs. (3) – (8), as a function of resistance
Q_{pred}	Capacity loss data as predicted by the model described by Eqs. (10)–(13), as a function of resistance

data with resistance increase values greater than 25% was removed, since the experimental campaign in [1] only tested cells up to this limit. Therefore, any generated synthetic data past this limit may have been less reliable.

3. Proposed methodology

The proposed methodology involves estimation of critical battery variables such has SOC, internal resistance, battery capacity, and the RUL and it is built upon a scheme that is a combination of a model-based estimator and a stochastic health prediction model as shown in Fig. 2a.

The model-based estimator is a particle filter. This was chosen due to its superior performance for nonlinear and non-Gaussian systems. The particle filter is tasked with the duties of estimating the SOC and internal resistance of the battery. The internal resistance is a vital variable that provides knowledge about the extent of degradation in the voltage performance of the battery.

Further, the internal resistance estimated by the particle filter is used by the stochastic health prediction models that are developed using the experimental data described in Section 2. The health prediction model consists of a capacity fade estimation model and a RUL prediction model. Together, it provides capacity estimates at any given instance with 95% confidence intervals, and the cycle life in terms of Ampere-hour throughput remaining before the battery reaches its EOF. This approach is different from the semi-empirical capacity fade model proposed in [1] in several respects. First, both the capacity loss and RUL algorithms in this work are stochastic, while the semi-empirical model is deterministic and only estimates capacity loss. Second, the proposed model is developed from a novel relationship between capacity and resistance (see Section 6). This correlation is simple yet effective for prediction, thus providing computational advantages over much more complex state of health models such as the semi-empirical capacity fade model.

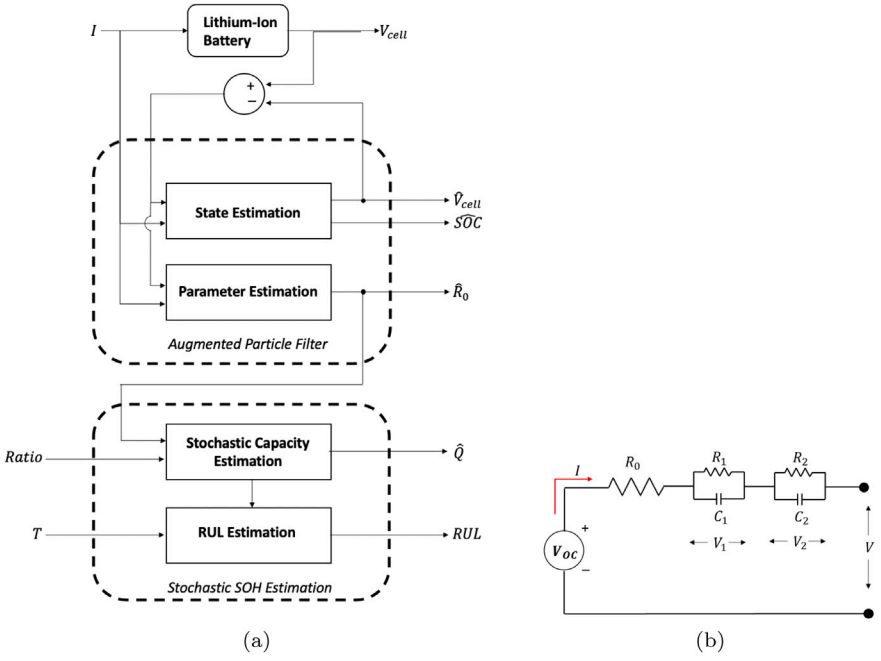

Fig. 2. (a) Combined SOH estimation and prognostic scheme, and (b) Schematic of a second-order Equivalent Circuit Model for a lithium-ion battery.

4. Battery model

A second-order equivalent circuit model (ECM), as shown in Fig. 2b, is employed to predict the dynamics of a lithium-ion battery.

The model is composed of an open circuit voltage source (V_{OC}) connected in series with a high-frequency internal resistance (R_0), and two RC pairs (R_1, C_1; R_2, C_2) that replicate the charge transfer and diffusion dynamics of the battery. The internal resistance R_0 is assumed to depend on the battery SOC, whereas the remaining model parameters are assumed constant across the entire operating range of the battery SOC [25]. The SOC is computed using the Coulomb counting method. It is worth noting that the internal resistance R_0 of the battery model is known to be higher at lower temperatures. However, in the present work the temperature dependence is not explicitly accounted for due to lack of experimental data. Instead, this work focuses on establishing an estimation framework for a battery model to aid the stochastic prediction of SOH and RUL. The battery model used in this paper can be updated with explicit temperature dependencies in its model parameters if experimental data at various temperatures is available, without making changes to the scheme proposed in Section 3. The discrete-time equations describing the dynamics of the second-order ECM are given below

$$\begin{cases} SOC(k+1) &= SOC(k) - \dfrac{\Delta t}{Q_0} I(k) \\ V_1(k+1) &= e^{\frac{-\Delta t}{R_1 C_1}} V_1(k) + R_1 \left(1 - e^{\frac{-\Delta t}{R_1 C_1}}\right) I(k) \\ V_2(k+1) &= e^{\frac{-\Delta t}{R_2 C_2}} V_2(k) + R_2 \left(1 - e^{\frac{-\Delta t}{R_2 C_2}}\right) I(k), \end{cases} \tag{5}$$

where Q_0 is the battery nominal capacity, Δt is the sampling time, $I(k)$ is the input current, and k is the discrete time step. Using Kirchhoff's voltage law, the terminal voltage of the battery is expressed as:

$$V_{cell}(k) = V_{OC}(SOC(k)) - V_1(k) - V_2(k) - R_0(SOC(k))I(k). \tag{6}$$

The discrete-time nonlinear state-space representation of the above equivalent circuit model is then given by

$$\begin{cases} x(k+1) &= Ax(k) + Bu(k) \\ y(k) &= g\left(x(k), u(k)\right), \end{cases} \tag{7}$$

where the state vector is $x(k) = [SOC(k) \quad V_1(k) \quad V_2(k)]^T$, the input is $u(k) = I(k)$, the output variable is $y(k) = V_{cell}(k)$, $g(x(k), u(k))$ is the nonlinear function expressed in the right hand side of (6), and the matrix $A \in \mathbb{R}^{3\times3}$ and column vector $B \in \mathbb{R}^{3\times1}$ are as given below

$$\begin{cases} A = \begin{bmatrix} 1 & 0 & 0 \\ 0 & e^{\frac{-\Delta t}{R_1 C_1}} & 0 \\ 0 & 0 & e^{\frac{-\Delta t}{R_2 C_2}} \end{bmatrix} \\ B = \begin{bmatrix} -\dfrac{\Delta t}{Q} \\ R_1 \left(1 - e^{\frac{-\Delta t}{R_1 C_1}}\right) \\ R_2 \left(1 - e^{\frac{-\Delta t}{R_2 C_2}}\right) \end{bmatrix}. \end{cases} \tag{8}$$

4.1. Identification and validation results

The model parameters are identified by fitting the model's output voltage to the experimentally measured voltage data. A Hybrid Pulse Power Characterization (HPPC) profile is used for the identification procedure. The cell is fully charged to 100% SOC before subjecting it to the HPPC profile at a temperature of 30 °C. The HPPC profile is composed of a train of discharge and charge pulses at every 10% SOC interval. The cell is discharged all the way down to approximately 7% SOC. A global optimization algorithm, the Particle Swarm Optimization, is utilized to minimize the objective function, which is the RMSE between the model-predicted and measured voltage. The identification results are shown in Fig. 3a with a voltage RMSE of 10.6 mV.

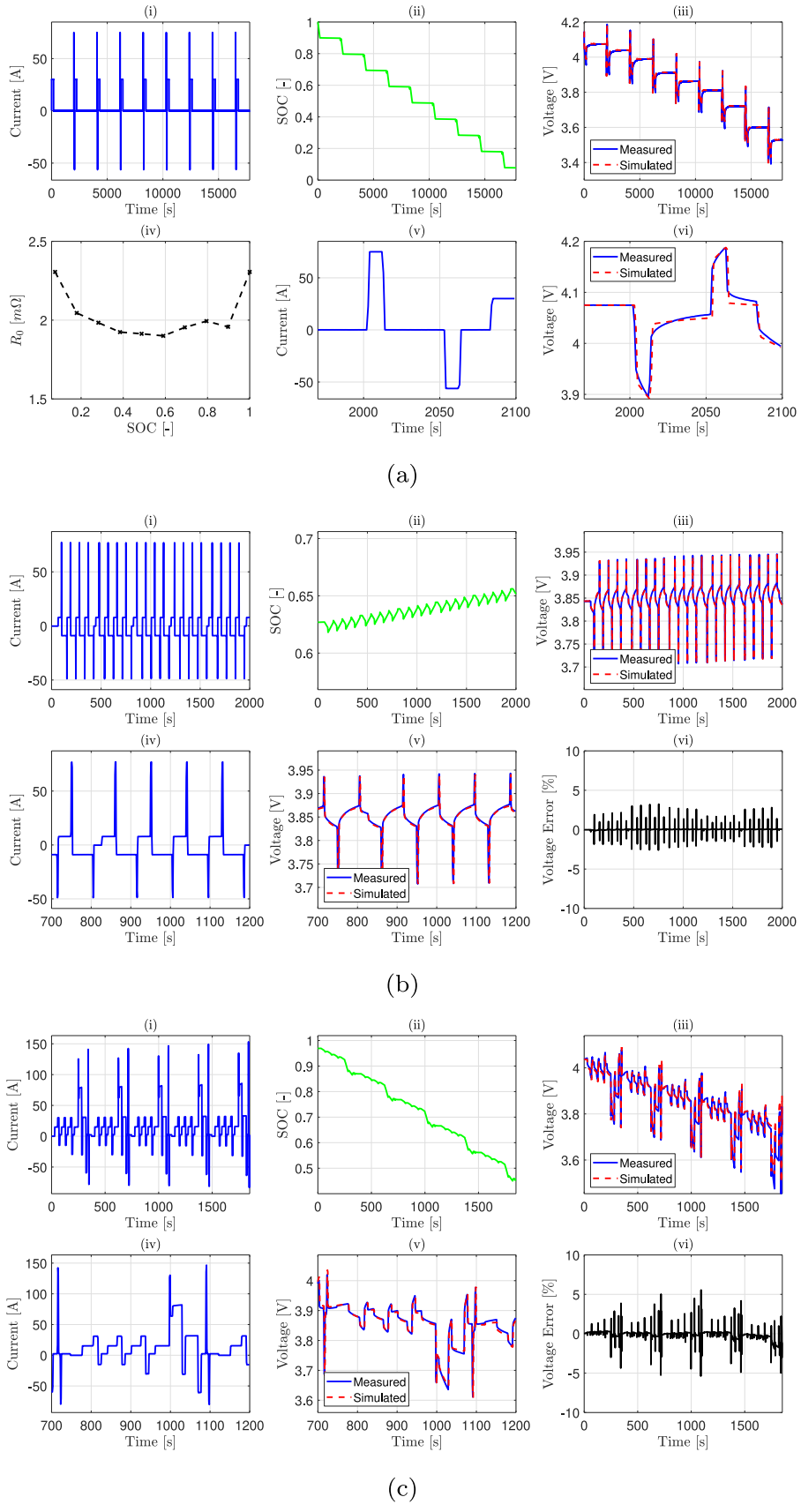

Fig. 3. Identification and validation results for the (a) HPPC, (b) charge sustaining, and (c) charge depleting current profiles. The plots contain: measured current, SOC profile, voltage response comparison between model and measured data, identified internal resistance R_0 as a function of SOC, zoom-in of the current and voltage profiles, and the percentage voltage error plot.

Further, to verify the performance of the battery model, its predictive performance is validated against two dynamic current profiles. First is a charge-sustaining current profile that has minimal deviation in terms of SOC. The voltage RMSE reported for this profile is 15.6 mV, and the plots are shown in Fig. 3b. Next, the model is validated against a charge depleting profile, spanning a larger range of SOC. The corresponding current profile and voltage response validation plots are shown in Fig. 3c, and the voltage RMSE is calculated to be 26.2 mV.

5. Particle filter

Particle filters [26,27] are well suited for the estimation of state variables of nonlinear and non-Gaussian systems. The particle filter used in this work is based on a Sequential Monte Carlo method that uses recursive Bayesian filtering to estimate the internal states/parameters of a system modeled as below

$$\begin{cases} x(k) &= f(x(k-1), u(k-1)) + w(k) \\ y(k) &= g(x(k), u(k)) + v(k), \end{cases} \tag{9}$$

where $x(k) \in \mathbb{R}^n$, $u(k) \in \mathbb{R}^p$, $y(k) \in \mathbb{R}^m$ are the state, input, and output variables, respectively. Further, $w(k) \in \mathbb{R}^n$ and $v(k) \in \mathbb{R}^m$ are the process and measurement noise, respectively. The nonlinear function mapping is described as $f : \mathbb{R}^n \times \mathbb{R}^p \to \mathbb{R}^n$ and $g : \mathbb{R}^n \times \mathbb{R}^p \to \mathbb{R}^m$.

Most of the estimation work found in the literature makes use of Kalman filters, such as the Sigma-point Kalman Filter or the Extended Kalman Filter (EKF), where the process and measurement noise are assumed to be Gaussian [28]. The EKF, which is widely used in the literature for battery state estimation, utilizes the Jacobian to linearize the nonlinear dynamics thereby introducing approximation errors. On the other hand, the particle filter handles non-Gaussian noise and preserves the system nonlinearities. Despite providing accurate estimates, the particle filter is known to be computationally intensive. However, in this work, given that the number of states and parameters to be estimated are only four, coupled with the fact that advancement in micro-controllers and computing speeds has enabled designers to use computationally expensive algorithms, the proposed methodology employs a particle filter with the knowledge that it can be substituted by other estimation algorithms in the presence of computational constraints with a trade-off in accuracy. The design steps of a particle filter for a general nonlinear system given in (9) are illustrated below:

1. **Initialization**: Randomly draw N particles of the state vector $x_1(k), x_2(k), \dots, x_N(k)$ at time step k, where each particle $x_i \in \mathbb{R}^n$ and $i = 1$ to N denotes the particle number.
2. **Prediction**: Each particle $x_i(k)$ is passed through a nonlinear stochastic state transition and measurement model (such as the one in (9)) to predict the state and output for the next time step. Let the predicted state vector and output be denoted as $\hat{x}_i^-(k)$ and $\hat{y}_i(k)$ given by

$$\begin{cases} \hat{x}_i^-(k) &= f(x_i(k-1), u(k-1)) + w(k) \\ \hat{y}_i(k) &= g(x_i(k), u(k)) + v(k). \end{cases} \tag{10}$$

3. **Correction**: The predicted outputs $\hat{y}_i(k)$ are compared with the experimentally measured value $y(k)$ to determine which particles are more likely to represent the true value. This is equivalent to assessing the conditional probability of seeing the measurement $y(k)$ given the predicted state $\hat{x}_i^-(k)$ and output $\hat{y}_i(k)$, respectively, are the true values. The conditional probability $q_i(k)$ is expressed as

$$q_i(k) = p\left(y(k) | \hat{x}_i^-(k)\right), \tag{11}$$

wherein, under the assumption of a Gaussian sensor measurement noise given by $v \sim \mathcal{N}\left(0, \sigma^2\right)$, the conditional probability is

$$q_i(k) = \frac{1}{\sigma\sqrt{2\pi}} \exp\left[-\frac{\left(y(k) - \hat{y}_i(k)\right)^2}{2\sigma^2}\right]. \tag{12}$$

In addition, based on the conditional probability, a normalized weight $W_i(k)$ is assigned to each particle to indicate the likelihood that the particle represents the real values. This is given as:

$$W_i(k) = \frac{q_i(k)}{\sum_{i=1}^N q_i(k)}, \tag{13}$$

where $\sum_{i=1}^N W_i(k) = 1$.

4. **Resampling and State Estimation**: The particles are then resampled based on the normalized weights to generate a new set of N state particles $x_1(k), x_2(k), \dots, x_N(k)$, wherein the highly weighted particles are chosen repeatedly. The *corrected* state estimate is denoted as $\hat{x}_i^+(k)$ and computed by taking the mean of the resampled particles as expressed below

$$\hat{x}_i^+(k) = \frac{1}{N}\sum_{i=1}^N x_i(k). \tag{14}$$

5. **Iteration**: The set of new resampled particles $x_1(k), x_2(k), \dots, x_N(k)$ are then propagated to the next time step by setting the time step as $k = k + 1$, and returning to step 2.

5.1. Particle filter implementation

In this work, the particle filter is employed for the combined estimation of state and parameter of the battery model described in Section 4. The main objective of the particle filter is to estimate the SOC (state) and the internal resistance R_0 (parameter). The particle filter is developed for an augmented state-space representation of the model given by

$$\begin{cases} x_{aug}(k) &= A_{aug}x_{aug}(k) + B_{aug}u(k) + w(k) \\ y(k) &= g(x_{aug}(k), u(k)) + v(k), \end{cases} \tag{15}$$

where the augmented state vector is $x_{aug}(k) = [SOC(k)\ V_1(k)\ V_2(k)\ R_0]^T$, $w(k) = [w_1(k)\ w_2(k)\ w_3(k)\ w_4(k)]^T$, $v(k) \in \mathbb{R}$, and the matrices are expressed as

$$\begin{cases} A_{aug} = \begin{bmatrix} 1 & 0 & 0 & 0 \\ 0 & e^{\frac{-\Delta t}{R_1C_1}} & 0 & 0 \\ 0 & 0 & e^{\frac{-\Delta t}{R_2C_2}} & 0 \\ 0 & 0 & 0 & 1 \end{bmatrix} \\ B_{aug} = \begin{bmatrix} -\frac{\Delta t}{Q} \\ R_1\left(1 - e^{\frac{-\Delta t}{R_1C_1}}\right) \\ R_2\left(1 - e^{\frac{-\Delta t}{R_2C_2}}\right) \\ 0 \end{bmatrix}. \end{cases} \tag{16}$$

The dynamics of the parameter is considered to be slowly varying such that: $R_0(k+1) = R_0(k) + w_4(k)$. This assumption is valid since the internal resistance varies slowly over the course of battery's lifetime.

The performance of the model-based estimator is verified against the dynamic charge depleting current profile. Since the internal resistance of the cell increases as the battery ages, the performance is tested over the entire lifespan of the battery at different Ah throughput values. Cell #7 from Table 1 is chosen to validate the estimator's performance. The operating conditions for Cell # 7 are: Ratio = 1; minimum SOC = 45%; Charging Rate (CR) = 3C/2. The combined estimation of SOC and R_0 is shown in 4a for a charge depleting current profile. The results are for a stage when the cell has been significantly aged, wherein

Table 4
Comparison of estimated increase in resistance $\hat{R}_{inc}$ with the resistance increase R_{inc} from the aging model in [1] for Cell # 7.

Data point	Amperehour throughput [Ah]	Model R_{inc} [%]	Estimated $\hat{R}_{inc}$ [%]
1	3791.6	2.39	2.97
2	9807	6.19	6.79
3	21921.3	13.84	12.22
4	24 000	15.15	16.58

an Ampere-hour throughput of 24 000 Ah has been extracted from the cell. The estimated SOC is compared with the reference SOC computed using the Coulomb counting method. It is observed that the estimated SOC tracks the reference SOC despite an incorrect initialization. On the other hand, the estimated resistance is filtered to smooth out the transients and plotted against the reference resistance computed by scaling the identified $R_0(SOC)$ in Fig. 3a by R_{inc}[%] from the aging model in [1]. Further, the SOC and resistance R_0 estimation plots at various Ampere-hour throughput are shown in 4b demonstrate a good performance over the entire lifespan of the battery. Note that in a real BMS, the final SOC at the end of the drive cycle may vary, and hence the average of the estimated resistance over an entire drive cycle can also be used as good estimate. In addition, at the end of the drive cycle, the increase in estimated resistance ($\hat{R}_{inc}$[%]) of the cell is computed using (3), which is compared to the R_{inc}[%] from the model in [1] and presented in Table 4. The estimated $\hat{R}_{inc}$ values are then fed to the stochastic capacity loss model described in the next section.

6. Capacity loss model

The proposed model predicts capacity loss as the sum of a deterministic and a stochastic term. The deterministic term is in the form of a square-root equation derived from an initial data fitting of capacity loss with respect to resistance increase, whereas the stochastic term is from fitting a Gaussian distribution to the error of this square-root fit.

Capacity loss and internal resistance growth are conventionally viewed as independent functions of time, ampere-hour throughput or certain operating conditions such as depth of discharge [29]. In this study, we exploit the functional relationship between capacity and resistance and use it to predict capacity loss primarily from dynamic online estimation of resistance increase through the particle filter. Experimental data were used to generate a capacity loss against resistance plot, which exhibited clear square root trends as shown in Fig. 5a.

In developing the proposed prognostic algorithm, grouping the data by cell Ratio was shown to be a promising approach for more accurate estimates of capacity loss. MATLAB's $polyfit$ function was used to calculate the best fit square root equations for capacity loss data, Q_{exp}, grouped by Ratio, along with the 95% confidence error bound calculated using MATLAB's $polyval$ function, describing the range that approximately 95% of the data is estimated to be within. The prediction of capacity loss using the square-root fitted equation is a relatively accurate initial, non-stochastic estimate defined as

$$Q_{ratio} = \begin{cases} 2.6964\sqrt{(R_{syn})} + 0.5403, & Ratio = 1 \\ 2.2870\sqrt{(R_{syn})} + 0.4467, & Ratio = 1/2 \\ 1.9636\sqrt{(R_{syn})} + 0.3726, & Ratio = 1/4. \end{cases} \quad (17)$$

In the prediction model development stage, the raw error E_{raw}, defined as $E_{raw} = Q_{ratio}(R_{syn}) - Q_{syn}$, is used which indicates the difference between the deterministic prediction Q_{ratio} as given by (17) and the Q_{syn}.

75% of the generated data for each Ratio was used to train the model, while the other 25% was used to test it. All of the experimental data available for each Ratio was used to train the model. Table 5 details how the experimental and generated data were used to build the proposed model.

The overall stochastic life prediction model is given by

$$Q_{pred} = Q_{ratio}(R_{syn}) + \omega, \quad (18)$$

where ω is the stochastic term with normal distribution, i.e. $\omega \sim \mathcal{N}(\mu, \sigma^2)$, with

$$\mu = \begin{cases} 0.6015, & Ratio = 1 \\ 0.4943, & Ratio = 1/2 \\ 0.4139, & Ratio = 1/4 \end{cases} \quad (19)$$

$$\sigma = \begin{cases} 0.4652, & Ratio = 1 \\ 0.3906, & Ratio = 1/2 \\ 0.3336, & Ratio = 1/4. \end{cases} \quad (20)$$

The stochastic feature of the model is expressed in terms of the mean and standard deviation of the error normal distribution which is fitted to the E_{raw} for an initial prediction of capacity loss using (17). The E_{raw} is plotted as a histogram (grouped by Ratio), and shown in Fig. 6 for $Ratio = 1$. A normal distribution for each Ratio is fitted to these histograms, and its mean (μ) and standard deviation (σ) are calculated as specified in (19) and (20).

Thus, the final capacity loss model equations are characterized as per the Ratios, and the Gaussian noise (mean and standard deviation), too, are described as a function of Ratios.

Since (18) predicts a small percent capacity loss (between 0.3% and 0.6%) at the beginning of life when resistance has not increased, the use of the stochastic term serves to mitigate this effect by subtracting away the majority of this initial error.

6.1. Capacity loss model validation

The accuracy of the capacity loss model is assessed via the modeling error:

$$E_{mod}(Q_{pred}, Q_{syn}) = Q_{pred} - Q_{syn}. \quad (21)$$

The RMSE of E_{mod} is calculated as $RMSE = \sqrt{\frac{\sum_{i=1}^{j} E_{mod,i}^2}{j}}$, where j is the total number of synthetic data used to validate the model, wherein $E_{mod} \in \mathbb{R}^j$.[2]

The model has an average RMSE of 0.9124 percent capacity loss when tested on the validation data (see Table 5), with the RMSE for each Ratio being: 1.0707 for Ratio 1, 0.8886 for Ratio 1/2 and 0.7490 for Ratio 1/4.

The difference in RMSE between Ratios can likely be explained by the variation of the experimental Q_{exp} data, which contained 8 cells of data for Ratio 1 but only 3 cells total for both Ratio 1/2 and Ratio 1/4. The Ratio 1 data set naturally had a larger amount of noise than those of the other Ratios, which could have led the model which was used to generate Q_{syn} data to produce a greater spread of values for Ratio 1.

To summarize, the proposed capacity loss model is able to accurately predict capacity loss within one percent capacity loss, from resistance and Ratio data. In an on-board application, resistance can be calculated using model-based adaptive observers, while Ratio can be tracked using the vehicle's battery management system.

7. Remaining useful life model

In addition to the capacity loss model, a separate model for the prediction of RUL was developed on the same data sets (see Table 5). Since charge throughput can be calculated on-board via current integration, the objective of this model is to estimate the charge throughput at the

[2] j is 25% of the overall synthetic data set, which is approximately 64,000 data points.

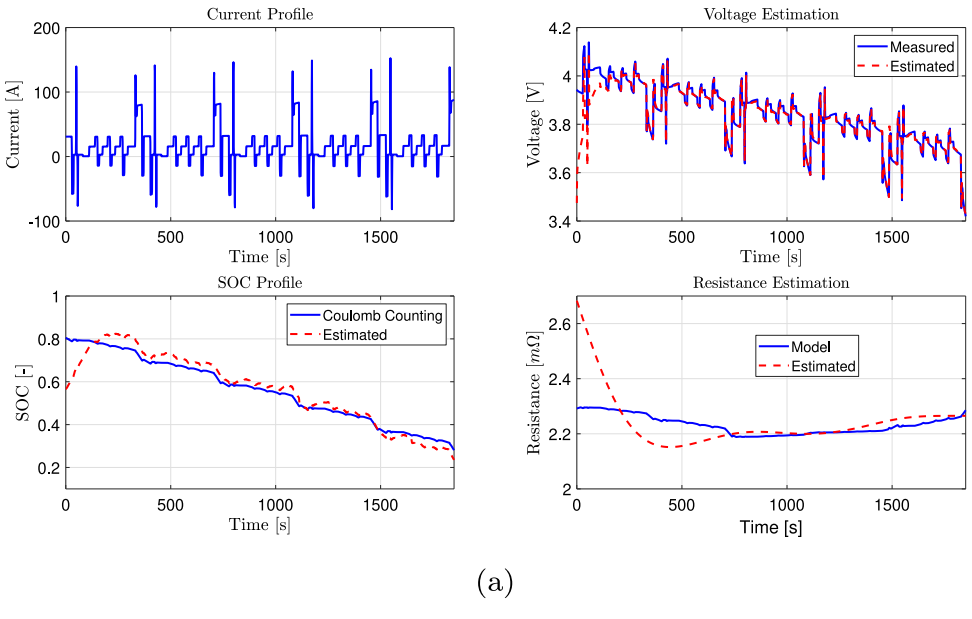

Fig. 4. The combined estimation results from the particle filter for Cell # 7 for a charge depleting current profile : (a) after extracting an Ampere-hour throughput of 24 000 Ah, with plots for voltage estimation (top right), SOC estimation (bottom left), and R_0 estimation (bottom right), and (b) at different Ah throughput during different stages of Cell # 7's lifespan.

Table 5
Description of the data used in the capacity loss model development and validation. Data for building the model is generally referred to as Q_{syn} even though it includes some Q_{exp} data.

Ratio	Data for building model	Data for validating model
$Ratio = 1$	8 cells of Q_{exp} data with Ratio 1 and 75% of the Q_{syn} data with Ratio 1	25% of Q_{syn} data with Ratio 1
$Ratio = 1/2$	2 cells of Q_{exp} data with Ratio 1/2 and 75% of Q_{syn} data with Ratio 1/2	25% of Q_{syn} data with Ratio 1/2
$Ratio = 1$	1 cell of Q_{exp} data with Ratio 1/4 and 75% of the Q_{syn} data with Ratio 1/4	25% of Q_{syn} data with Ratio 1/4

EOL. With this estimate, RUL (measured in Ah), can then be calculated dynamically and on-board using the equation

$$RUL = Amph_{EOL} - Amph(t), \tag{22}$$

where $Amph_{EOL}$ is the charge throughput at EOL and $Amph(t)$ is the charge throughput value at time t.

After testing for trends between operating conditions, capacity loss, and charge throughput, it was found that temperature had a statistically significant correlation with capacity loss and charge throughput. The data was separated by Ratio, as also done for the development of the capacity loss model. Of the two other operating conditions which were analyzed, C-rate had no correlation whatsoever, while SOC_{min} only had minimal correlation (but not statistically significant enough for it to be included in the model). The three plots in Fig. 7 describe capacity loss as a function of charge throughput and SOC_{min} (top), C-rate (middle) and Temperature (bottom), respectively. It is observed that temperature has a clear relationship with capacity loss and charge

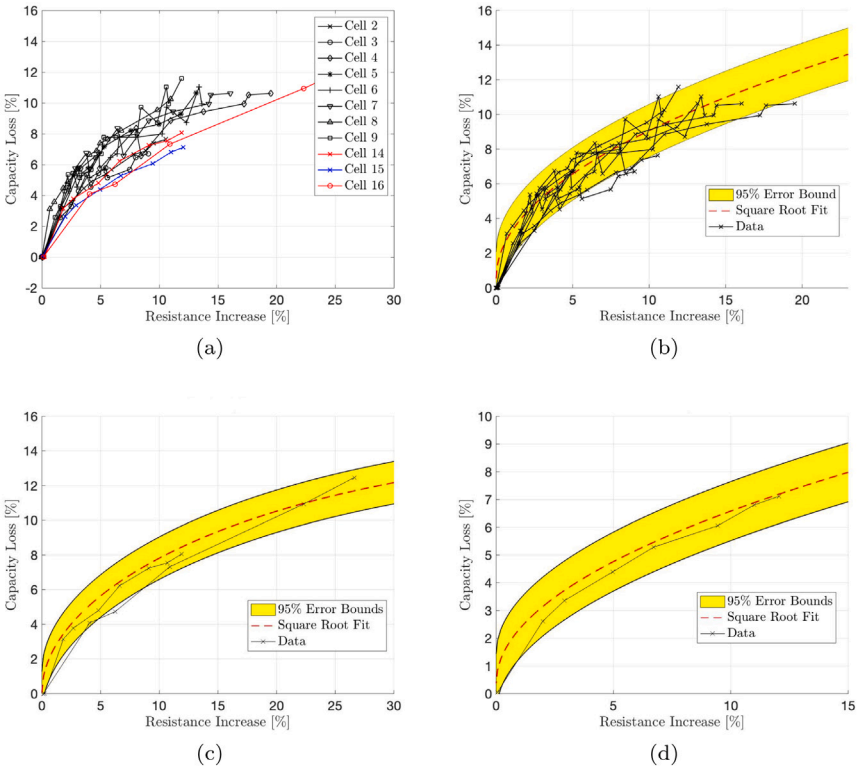

Fig. 5. (a) Experimental capacity loss (Q_{exp}) plotted against resistance increase, color-coded by Ratio: Ratio 1 in black, Ratio 1/2 in red, and Ratio 1/4 in blue for the experiments of Table 1; Q_{exp} data with best-fit square root equations and error bounds for Ratio 1 (b), Ratio 1/2 (c), and Ratio 1/4 (d). (For interpretation of the references to color in this figure legend, the reader is referred to the web version of this article.)

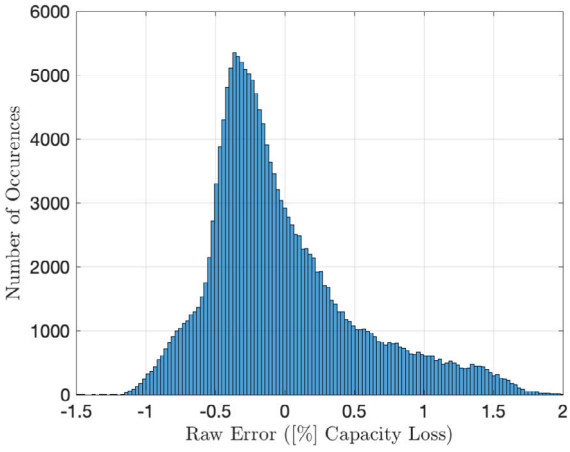

Fig. 6. The histogram of raw error for Ratio 1 data.

throughput, while the trajectories of charge throughput vs. capacity loss are almost completely independent of SOC_{min} and C-rate.

The predicted RUL, denoted as RUL_{pred}, is defined through the polynomial function P_{ratio} expressed as $P_{ratio}\left(\hat{Q}_{syn}, \hat{T}\right)$, where $\hat{Q}_{syn}$ and $\hat{T}$ are the normalized values of Q_{syn} and T, respectively. Note that normalizing the data by its mean and standard deviation avoids computational burden associated with extremely small or large numbers, and provides accurate estimates of the coefficients for the equation of the fitted surface. In particular, $\hat{T}$ is computed as

$$\hat{T} = \frac{T - 310}{4.546}, \tag{23}$$

for all Ratios given that the range of temperature data is always the same. Conversely, Q_{syn} values vary across Ratios and thus are normalized differently based on the fitting used, producing different $\hat{Q}_{syn}$ values for each Ratio given by

$$\hat{Q}_{syn} = \begin{cases} \dfrac{Q_{syn} - 9.243}{3.564}, & Ratio = 1 \\ \dfrac{Q_{syn} - 7.833}{3.029}, & Ratio = 1/2 \\ \dfrac{Q_{syn} - 6.719}{2.607}, & Ratio = 1/4. \end{cases} \tag{24}$$

It follows that the predicted RUL can be expressed as

$$RUL_{pred} = P_{ratio}\left(\hat{Q}_{syn}, \hat{T}\right), \tag{25}$$

where the polynomial model P_{ratio} for different Ratios are given below

$$\begin{cases} P_{ratio}\left(\hat{Q}_{syn}, \hat{T}\right)|_{Ratio=1} = & 13750 + 10760\hat{Q}_{syn} - 3548\hat{T} + 1442\hat{Q}_{syn}^2 - \\ & 2109\hat{Q}_{syn}\hat{T} + 441.3\hat{T}^2 - 307.4\hat{Q}_{syn}^3 - \\ & 188.7\hat{Q}_{syn}^2\hat{T} + 245.8\hat{Q}_{syn}\hat{T}^2 \\ P_{ratio}\left(\hat{Q}_{syn}, \hat{T}\right)|_{Ratio=1/2} = & 13910 + 10790\hat{Q}_{syn} - 3528\hat{T} + 1195\hat{Q}_{syn}^2 - \\ & 1882\hat{Q}_{syn}\hat{T} + 394.7\hat{T}^2 - 408.1\hat{Q}_{syn}^3 - \\ & 70.6\hat{Q}_{syn}^2\hat{T} + 213.6\hat{Q}_{syn}\hat{T}^2 \\ P_{ratio}\left(\hat{Q}_{syn}, \hat{T}\right)|_{Ratio=1/4} = & 14090 + 10830\hat{Q}_{syn} - 3507\hat{T} + 932\hat{Q}_{syn}^2 - \\ & 1634\hat{Q}_{syn}\hat{T} + 342.1\hat{T}^2 - 514.4\hat{Q}_{syn}^3 - \\ & 60.5\hat{Q}_{syn}^2\hat{T} + 176.3\hat{Q}_{syn}\hat{T}^2. \end{cases} \tag{26}$$

The RUL model was tested on the Q_{syn} training data set and the error, i.e. $E_{RUL} = RUL_{pred} - RUL_{syn}$, where RUL_{syn} is the RUL of the experimental or synthetic data point. The histogram of the RUL error, shown in Fig. 8, does not fit any known distribution to properly capture the spread of the data. Clearly, the model underestimates RUL leading

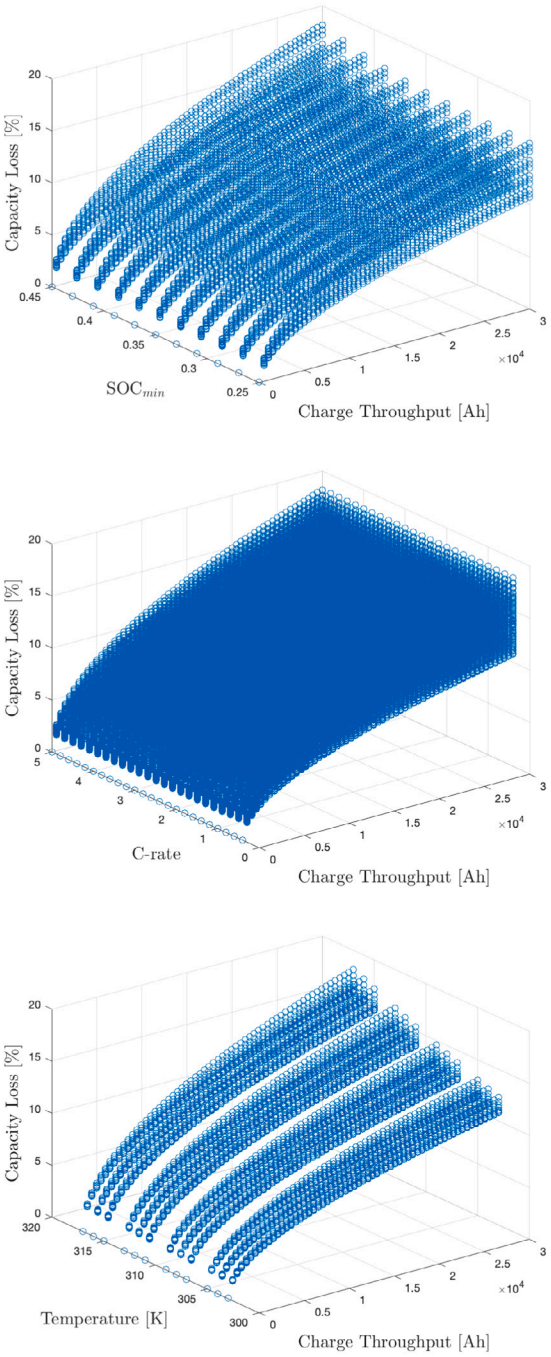

Fig. 7. Capacity loss and charge throughput correlation with SOC_{min} (top), C-rate (middle), and Temperature (bottom). Temperature shows a clear relationship with those two variables—as temperature increases, capacity is lost at a faster rate. Shown here is the data for Ratio 1, but other Ratios had very similar results.

to a significant bias as observed from the negative raw error values in Fig. 8.

To offset this bias, the mean raw error, referred to as $\bar{e}$, is calculated and subtracted from all predictions as

$$RUL_{pred} = P_{ratio}\left(\hat{Q}_{syn}, \hat{T}\right) - \bar{e}, \tag{27}$$

where the values of $\bar{e}$ are reported below

$$\bar{e} = \begin{cases} -1045 \text{ Ah}, & Ratio = 1 \\ -1341 \text{ Ah}, & Ratio = 1/2 \\ -1644 \text{ Ah}, & Ratio = 1/4. \end{cases} \tag{28}$$

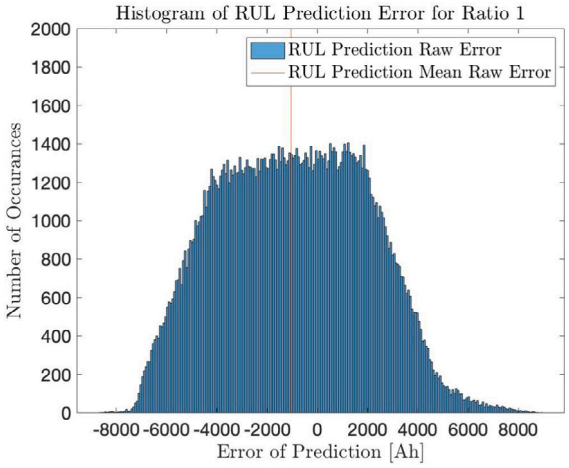

Fig. 8. The histogram of the raw error of the RUL model in (23)–(26), which demonstrates how the model consistently underpredicts RUL.

The RUL model's error improved significantly producing an RMSE of 1984 Ah when validated on the Q_{syn} validation data set using the model in (23)–(26), while the RMSE of RUL prediction decreased to 1604 Ah. Normalizing the latter RMSE with respect to the average life of a cell in the data (roughly 30,000 Ah), the new percentage RMSE for predicting RUL is 5.33%.

In summary, the RUL model accurately estimates the remaining charge throughput until EOL, given percent capacity loss and temperature as inputs. The former may be calculated through the aforementioned stochastic capacity loss model, while the latter is easy to measure online. The exclusion of operating conditions SOC_{min} and C-rate from this model aligns with the experimental data and literature, as the model that was used to generate synthetic data behaves similarly and also exhibits low C-rates (see (4)).

8. Combined results: Model-based estimator, stochastic capacity loss and RUL model

The proposed estimation scheme, which combines the strengths of model-based estimation with data-driven stochastic health prediction, is validated for Cell #7 (see Table 6) through different stage of its life.

As described in Section 5, the battery is subjected to a dynamic current profile during the different stages of health, and the resulting current and voltage measurements are used as an input to the model-based estimator. Four data points at different battery Ampere-hour throughput are selected as shown in column 2 of Table 6. The particle filter developed for the equivalent circuit model uses the measured current and voltage data to estimate the battery SOC and resistance increase. The resistance increase values from the aging model in [1] and the estimated values from the particle filter are compared in columns 3 and 4 of Table 6. Next, the estimated resistance increase values are input to the stochastic model to predict the capacity loss values. The measured capacity loss values and the predicted values from the stochastic model are listed in columns 5 and 6 of Table 6. Further, the model and estimated RUL values are listed in column 7. As observed in Table 6, the accuracy of the estimated capacity loss and RUL values improves as the battery ages.

9. Conclusions

A stochastic prognostic model for capacity loss and remaining useful life in lithium-ion batteries with NMC–LMO chemistry has been developed. The stochastic health prediction model works in conjunction with a model-based estimator, developed using a particle filter

Table 6
Comparison of predicted R_{inc}, Q_{loss}, and RUL with experimental results. Predictions are from the holistic proposed model, including the particle filter, stochastic capacity loss algorithm, and RUL model.

Data point	Ah throughput [Ah]	Model R_{inc} [%]	Estimated $\hat{R}_{inc}$ [%]	Measured Q_{loss} [%]	Estimated Q_{loss} [%]	Measured RUL [Ah]	Estimated RUL [Ah]
1	3791.6	2.39	2.97	5.74	5.69	20208.4	20533.9
2	9807	6.19	6.79	8.34	8.83	14 193	15312.2
3	21921.3	13.84	12.22	10.52	10.14	2078.7	2476.3
4	24 000	15.15	16.58	10.62	10.78	0	48.2

for an equivalent circuit battery model, which estimates SOC and increasing resistance of the battery as it ages. The stochastic prognostic model was developed and validated on 11 cells of experimental data and over 250,000 synthetic data points. The model uses readily-measurable/estimated parameters or predetermined battery operating conditions such as Ratio, temperature, and resistance and thus offers a convenient method for prediction. The particle filter estimates SOC and resistance, and the stochastic state of health algorithms are able to predict capacity loss within 1% and RUL within 1.6 kAh.

The stochastic aspect of the capacity fade model provides a mean to describe the variation of the capacity and resistance relationship via the Gaussian distribution and the calculation of the mean and standard deviation of error. The proposed methodology is computationally simple, probabilistic in nature (also providing error bounds), and offers room for physical explanation of the observed phenomena (as opposed to black box machine learning-based estimators). However, it should be noted that the scope of this model may be limited to the aging conditions used in the data. Nonetheless, the range of parameters used in this study were chosen to encompass the most common aging conditions. Moreover, the broader results of this work, such as the novel relationship between capacity and resistance as well as the finding that temperature influences EOL much more than C-rate or SOC_{min}, are valuable in and of themselves and merit further investigation. It should also be recognized that phenomena such as reversible capacity loss are not accounted for in this work [30–33]. Furthermore, since the proposed model provides error bounds which may encompass these uncertainties, the model holistically maintains its integrity.

Such a model, which can accurately predict capacity loss, can be used to estimate when to replace lithium-ion batteries in PHEVs and effectively extend the lives of these batteries. In addition, this model could also be incorporated into on-board battery management systems to provide drivers with real-time feedback on how to mitigate aging by changing their driving behavior.

Future work includes extending the proposed model to the pack level by accounting for cell-to-cell interactions and incorporating Arrhenius equation relating aging and temperature. Moreover, generalization of the aging conditions used in the data would help expand the utility of the model.

Declaration of competing interest

The authors declare that they have no known competing financial interests or personal relationships that could have appeared to influence the work reported in this paper.

Acknowledgment

Battery experiments were conducted at the Ohio State University Center for Automotive Research as part of the Industrial Consortium Research Program.

References

[1] A. Cordoba-Arenas, S. Onori, Y. Guezennec, G. Rizzoni, Capacity and power fade cycle-life model for plug-in hybrid electric vehicle lithium-ion battery cells containing blended spinel and layered-oxide positive electrodes, J. Power Sources 278 (2015) 473–483.
[2] R. Spotnitz, Simulation of capacity fade in lithium-ion batteries, J. Power Sources 113 (1) (2003) 72–80.
[3] J. Zhang, J. Lee, A review on prognostics and health monitoring of li-ion battery, J. Power Sources 196 (15) (2011) 6007–6014.
[4] L. Lam, P. Bauer, Practical capacity fading model for li-ion battery cells in electric vehicles, IEEE Trans. Power Electron. 28 (12) (2012) 5910–5918.
[5] P. Ramadass, B. Haran, R. White, B.N. Popov, Mathematical modeling of the capacity fade of li-ion cells, J. Power Sources 123 (2) (2003) 230–240.
[6] X. Hu, J. Jiang, D. Cao, B. Egardt, Battery health prognosis for electric vehicles using sample entropy and sparse Bayesian predictive modeling, IEEE Trans. Ind. Electron. 63 (4) (2015) 2645–2656.
[7] R. Xiong, Y. Zhang, J. Wang, H. He, S. Peng, M. Pecht, Lithium-ion battery health prognosis based on a real battery management system used in electric vehicles, IEEE Trans. Veh. Technol. 68 (5) (2018) 4110–4121.
[8] P. Spagnol, S. Onori, N. Madella, Y. Guezennec, J. Neal, Aging and characterization of li-ion batteries in a hev application for lifetime estimation, IFAC Proc. Vol. 43 (7) (2010) 186–191.
[9] L. Serrao, S. Onori, G. Rizzoni, Y. Guezennec, A novel model-based algorithm for battery prognosis, IFAC Proc. Vol. 42 (8) (2009) 923–928.
[10] E. Prada, D. Di Domenico, Y. Creff, J. Bernard, V. Sauvant-Moynot, F. Huet, A simplified electrochemical and thermal aging model of LiFePO4-graphite li-ion batteries: power and capacity fade simulations, J. Electrochem. Soc. 160 (4) (2013) A616.
[11] P. Tulpule, C.-Y. Chang, G. Rizzoni, Li-ion cell aging model online parameter estimation for improved prognosis, in: Dynamic Systems and Control Conference, Vol. 50695, American Society of Mechanical Engineers, 2016, V001T15A004.
[12] C.-Y. Chang, P. Tulpule, G. Rizzoni, W. Zhang, X. Du, A probabilistic approach for prognosis of battery pack aging, J. Power Sources 347 (2017) 57–68.
[13] A. Di Filippi, S. Stockar, S. Onori, M. Canova, Y. Guezennec, Model-based life estimation of li-ion batteries in PHEVs using large scale vehicle simulations: An introductory study, in: 2010 IEEE Vehicle Power and Propulsion Conference, 2010, pp. 1–6.
[14] R.D. Anderson, Y. Zhao, X. Wang, X.G. Yang, Y. Li, Real time battery power capability estimation, in: 2012 American Control Conference (ACC), IEEE, 2012, pp. 592–597.
[15] A. El Mejdoubi, H. Chaoui, H. Gualous, P. Van Den Bossche, N. Omar, J. Van Mierlo, Lithium-ion batteries health prognosis considering aging conditions, IEEE Trans. Power Electron. 34 (7) (2018) 6834–6844.
[16] C. Taborelli, S. Onori, State of charge estimation using extended Kalman filters for battery management system, in: 2014 IEEE International Electric Vehicle Conference (IEVC), IEEE, 2014, pp. 1–8.
[17] D. Di Domenico, A. Stefanopoulou, G. Fiengo, Lithium-ion battery state of charge and critical surface charge estimation using an electrochemical model-based extended Kalman filter, J. Dyn. Syst. Meas. Control 132 (6) (2010).
[18] F. Maletić, M. Hrgetić, J. Deur, Dual nonlinear Kalman filter-based soc and remaining capacity estimation for an electric scooter li-NMC battery pack, Energies 13 (3) (2020) 540.
[19] Z. Chen, J. Xiao, X. Shu, S. Shen, J. Shen, Y. Liu, Model-based adaptive joint estimation of the state of charge and capacity for lithium–ion batteries in their entire lifespan, Energies 13 (6) (2020) 1410.
[20] I.-S. Kim, A technique for estimating the state of health of lithium batteries through a dual-sliding-mode observer, IEEE Trans. Power Electron. 25 (4) (2009) 1013–1022.
[21] A. Allam, S. Onori, An interconnected observer for concurrent estimation of bulk and surface concentration in the cathode and anode of a lithium-ion battery, IEEE Trans. Ind. Electron. 65 (9) (2018) 7311–7321.
[22] W. Cai, J. Wang, Estimation of battery state-of-charge for electric vehicles using an MCMC-based auxiliary particle filter, in: 2016 American Control Conference (ACC), IEEE, 2016, pp. 4018–4021.
[23] E. Walker, S. Rayman, R.E. White, Comparison of a particle filter and other state estimation methods for prognostics of lithium-ion batteries, J. Power Sources 287 (2015) 1–12.
[24] A.A. Pesaran, T. Markel, H.S. Tataria, D. Howell, Battery Requirements for Plug-in Hybrid Electric Vehicles–Analysis and Rationale, Tech. rep., National Renewable Energy Lab.(NREL), Golden, CO (United States), 2009.
[25] R. Ahmed, J. Gazzarri, S. Onori, S. Habibi, R. Jackey, K. Rzemien, J. Tjong, J. LeSage, Model-based parameter identification of healthy and aged li-ion batteries for electric vehicle applications, SAE Int. J. Altern. Powertrains 4 (2) (2015) 233–247.
[26] M.S. Arulampalam, S. Maskell, N. Gordon, T. Clapp, A tutorial on particle filters for online nonlinear/non-Gaussian Bayesian tracking, IEEE Trans. Signal Process. 50 (2) (2002) 174–188.

[27] F. Gustafsson, Particle filter theory and practice with positioning applications, IEEE Aerosp. Electron. Syst. Mag. 25 (7) (2010) 53–82.
[28] R. Van Der Merwe, et al., Sigma-Point Kalman Filters for Probabilistic Inference in Dynamic State-Space Models (Ph.D. thesis), OGI School of Science & Engineering at OHSU, 2004.
[29] M. De Gennaro, E. Paffumi, G. Martini, A. Giallonardo, S. Pedroso, A. Loiselle-Lapointe, A case study to predict the capacity fade of the battery of electrified vehicles in real-world use conditions, Case Stud. Transp. Policy (2019).
[30] F. Benavente-Araoz, M. Varini, A. Lundblad, S. Cabrera, G. Lindbergh, Effect of partial cycling of NCA/Graphite cylindrical cells in different SOC intervals, J. Electrochem. Soc. 167 (2020).
[31] M. Lewerenz, P. Dechent, D.U. Sauer, Investigation of capacity recovery during rest period at different states-of-charge after cycle life test for prismatic $Li(Ni_{1/3}Mn_{1/3}Co_{1/3})O_2$-graphite cells, J. Energy Storage 21 (2019) 680–690.
[32] M. Lewerenz, G. Fuchs, L. Becker, D.U. Sauer, Irreversible calendar aging and quantification of the reversible capacity loss caused by anode overhang, J. Energy Storage 18 (2018) 149–159.
[33] B. Epding, B. Rumberg, H. Jahnke, I. Stradtmann, A. Kwade, Investigation of significant capacity recovery effects due to long rest periods during high current cyclic aging tests in automotive lithium ion cells and their influence on lifetime, J. Energy Storage 22 (2019) 249–256.